Circuit Model for Graphene Screen-Printed Films

Circuit Model for Graphene Screen-Printed Films

Fabio Peinetti, Simone Quaranta, and Patrizia Savi

Abstract – Graphene flakes can be screen-printed on different substrates through the preparation of inks with a proper combination of solvents and binders. In this letter, an equivalent lumped circuit model of a graphene film is obtained by fitting the measured scattering parameters of a graphene-loaded microstrip lines with Cadence AWR software simulations.

1. Introduction

Films loaded with graphene nanoplatelets (GNPs) have gained great attention in the last decades. Through the preparation of inks with a proper combination of solvents and binders [1], films can be deposited on different substrates. The main techniques to deposit films are blade coating, ink jet [2, 3] and screen printing as described in details in [4]. Each technique requires proper ink preparation [5]. In particular screen printing calls for quite viscous and thixothropic pastes. Therefore a certain amount of binder/rheology modifier needs to be added to the paste formulation. Hence, the binder cannot be removed completely by thermal treatment when screen printing is performed on polymer -based substrates. Graphene films are used in many applications in the optical [6], RF and millimeter wavelength range as gas sensors [7], humidity sensors [8, 9], glucose sensors [10, 11], tunable devices [12, 13], flexible electronics [14, 15], and EM absorber [16]. In the case of films loaded with graphene, even if in many applications a graphene film can be easily described by using its sheet resistance, a customized model should be introduced in order to account for all the substances present in the deposition [17]. For what concern sensing applications, it would very helpful the characterization of graphene-based films with an electric equivalent circuit and the knowledge of the variation of the circuit parameters due to the interaction with the target molecules. Consequently, the knowledge of the electromagnetic properties of graphene at microwave frequency has become crucial. However, there has been little research carried out on the characterization of graphene films at microwave frequencies [18]. The circuit models at microwave frequency are generally based on series or paraller RLC resonators. In [16, 19] the authors introduce two models to describe graphene inks below (Davidson-Cole model) and above (Lorentz model) the percolation threshold. Two types of GNP-based inks were tested with 8 and 12 wt.% of poly(methyl methacrylate) (PMMA) in solution with organic solvent. In [20] is introduced an equivalent circuit of polyaniline polimeric matrix (PANI)/graphene nanocomposites formed by a parallel of a capacitor and a resistor, plus a series resistance taking into account the PANI.

In this letter, a description of graphene films with a lumped circuit model is introduced in which the binder and graphene are individually modeled. The model is obtained by fitting, in the microwave range, measured S-parameters on AWR software, from Cadence. Starting from the preliminary model described in [21], the binder and the graphene nanoplatelets are modeled individually. In the enhanced model of this work, the fitting of the parameters is greatly improved over the frequency range, and many circuit elements are added in order to deal with microscopic effects taking place at microwave frequency. The proposed equivalent lumped circuit model proves suitable as an initial step towards the full-wave electromagnetic modeling and analysis of graphene loaded microwave structures intended for sensing and tuning applications.

In Section 2 the microstrip circuit and film deposition are described. Section 3.1 deals with the model of the gap filled with a binder (ethyl-cellulose) film. In Section 3.2 the model of the film loaded with graphene flakes of weight fraction 25% and 33% is introduced. In Section 4 the measured S-parameters of the microstrip lines with binder alone and with graphene films are compared with the results obtained by the model.

2. Microstrip lines and film deposition

In order to obtain a circuit model of a film loaded with graphene, a simple microstrip line with a gap is considered (see Fig. 1). Across the gap, the ink with the chosen composition of graphene is deposited by screen-printing technique. In this work, graphene nanoplates by Nanoinnova (Spain) are used with a weight fraction of 25% and 33%. Screen printing paste was comprised of an ethyl cellulose (Sigma Aldrich, viscosity 10 cP, 5% toluene/ethanol, 48% ethoxyl) binder/stabilizer, α-terpineol solvent and graphene flakes as active ingredient. Component ratio (wt%) was 9.5:65.5:25, respectively. All components were mixed in ethanol stirred for 2h and finally sonicated with a titanium horn for 15h. Ethanol was removed by rotary-evaporation to attain a printable paste. Ink was deposited layer-by-layer by means of a 90T polyester screen printing mesh (Mismatic, Italy). Three layers were sequentially printed onto

an FR4 substrate achieve a 30 μm film thickness. Film dimensions measured up to 3 mm $\times$ 3 mm. The coating was dried at 125°C for 2.5 h [22].

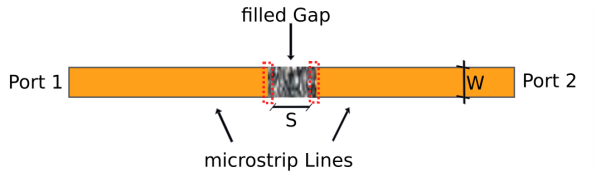

Figure 1: Top view of the microstrip line with a centered gap.

3. Circuit model of the film

First of all, instead of using the default microstrip gap element (MGAP) available in AWR with discrete components [23], a specific model of the gap is developed in order to obtain a better description of the percolative paths and of the losses in the dielectric. Furthermore, a series resistance,(R_s) successfully models the sheet resistance, measured in [7]. First, a model for the binder alone, Ethyl-Cellulose (EC), is developed (see Section 3.1). Then, based on this preliminary analysis, the final model describing the behavior of a graphene film with weight-fraction 25% is derived (see Section 3.2).

3.1. Binder-filled gap model

The default microstrip gap element (MGAP) available in AWR has some limitations on the dimensions of the gap ($0.1 < \mathrm{S/H} < 1$, $0.5 < \mathrm{W/H} < 2.5$) [23, 24]. In order to describe a gap with a geometry not included in the previously cited range (in our case S/H = 1.65 and W/H = 1.9 see Section 4) a new model of the binder-filled gap is introduced (see Fig. 2). The red-squared box is the "core", which is modified in order to fit graphene deposition's S-parameters (see Section 3.2) by adding other circuit elements. With respect to the classical model, made up of a capacitive pi-network [24], series resistors are added. A further variation includes the presence of an inductive element. In Fig. 2 the transmission lines connected to port 1 and port 2 are not shown. The inner capacitors toward ground (C_{gl}, C_{gr}), model the parallel plate capacitance between the microstrip connected to port 1 and port 2 and the ground plane, in correspondence of the gap. On the other hand, C_g accounts for the capacitance between the two lines, separated by the dielectric binder; C_g value is about 8 times lower than the capacitances C_{gl}, C_{gr} (see Table 1). We consider $C_{gl} = C_{gr}$. R_g, R_{gl} and R_{gr} account for losses in the dielectric at high frequency. Due to the high loss tangent, the corresponding resistance is in the order of a hundred

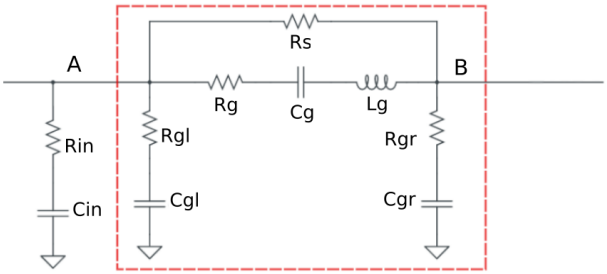

Figure 2: Binder-filled gap circuit.

Ohm. The resistor named R_s in Fig. 2, represents the sheet resistance and models the percolative path in the ethyl-cellulose filler. Since the binder matrix is basically dominated by the dielectric compound, the low efficient electron tunneling causes R_s to be large, namely 34 kΩ. As pointed out in several works (see e.g. [21, 22]), the real part of the impedance is influenced by variations in the actual composition of the compound: an increase in graphene weight fraction corresponds to a reduction of the resistance and vice-versa.

Table 1: Binder Electrical model parameters

R_s kΩ	R_g kΩ	C_g pF	L_g pH	R_{gl} Ω	C_{gl} pF	R_{gr} Ω
34	2.98	0.0107	15.8	91	0.085	91

C_{gr} pF	R_{in} Ω	C_{in} pF	R_{out} Ω	C_{out} pF	C_{pp} pF
0.085	3.4	0.38	–	–	–

3.2. Graphene-filled gap model

In this section the graphene weight fraction 25% and 33% film deposition are analyzed. Since the graphene ink requires an adhesion element, such as EC, to be printed and due to the impossibility to remove the binder, even with thermal treatment, the developed model accounts for both the effects of graphene and EC. This is the reason for which in Section 3.1, a model for the binder was developed. The circuital topology of Fig. 2 can be found in Fig. 3 (red box), too. However circuit parameters are changed in order to properly fit chemically different EC-graphene deposition as reported in Table 2 and Table 3. Moreover some components, placed inside the green box, are added to improve S-parameters fitting. In particular, the parallel capacitor C_{pp} accounts for the creation of nanoscale capacitors, whose conductive element is the graphene platelet and binder acts as dielectric material [21]. Moreover, an *RC* series element is added at the output node, making the circuit symmetric ($R_{in} = R_{out}$,

$C_{in} = C_{out}$). The increase in percolative paths is linked to a reduction in resistive elements and in particular in R_s, which falls from 34 kΩ to 425 Ω. The comparison of Table 1 and 2 shows that also the other resistors are strongly decreased. The same reasoning applies when increasing graphene weight fraction up to 33%; in this case R_s is further reduced to 207 Ω (see Table 3). The value of R_s can be used to evaluate the sheet resistance defined as:

$$R_{sheet} = R_s \frac{W}{S}. \quad (1)$$

The resulting sheet resistance is 425 Ω/□, using a unitary aspect ratio. The calculated value is a DC resistance between node A and node B, and it is very close to the measured value, namely 440 Ω/□, obtained in [21] with the same type of deposition. The inductance L_g, C_{gl} and C_{gr} are left unaltered as shown by Table 1 and 2 comparison.

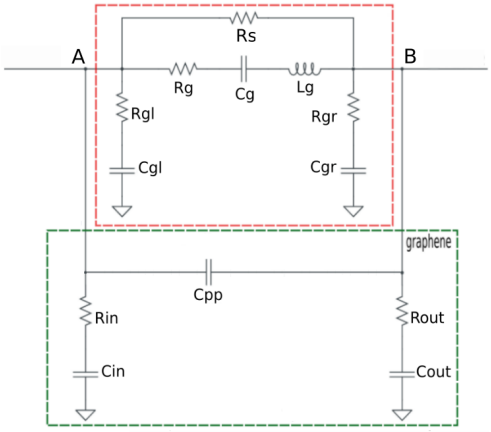

Figure 3: Graphene-filled gap circuit.

Table 2: Graphene weight fraction 25% Electrical model parameters

R_s kΩ	R_g kΩ	C_g pF	L_g pH	R_{gl} Ω	C_{gl} pF	R_{gr} Ω
0.425	1	0.032	15.8	28	0.085	28

C_{gr} pF	R_{in} Ω	C_{in} pF	R_{out} Ω	C_{out} pF	C_{pp} pF
0.085	36	0.2	36	0.2	0.029

4. Results

A 35 mm long copper microstrip line (corresponding to 50 Ω), was etched on FR4 substrate of thickness H = 1.57 mm, $\varepsilon_r = 3.9$, $\tan\delta = 0.03$, $\rho_{FR4} = 17.24$ mΩ · μm. The width (W) of the microstrip line was chosen to be 3 mm in order to have a 50 Ω impedance. A gap of length $S = 2.6$ mm, was left in the middle in order to host the graphene film (see Fig. 1). The size of the deposition was 3 mm × 3 mm, since 0.2 mm are over-imposed to the lines, on each side, in order to guarantee an electric connection (see Fig. 4) Three types of microstrip circuits were manufactured: one with an ink made with the binder alone and the other two with a deposition of two layers of graphene 25 wt.% ink and 33 wt.%. The scattering parameters of the microstrip lines with the film (binder alone and binder with graphene) were measured with a 2-port Vector Network Analyzer by Keysight (P9372A) from 200 MHz to 4.5 GHz. Fig. 5 shows the simulated S_{21} (solid lines), compared to the measured one (dashed lines) for the unfilled gap. The S-parameters remain unchanged when the gap is binder-filled because the relative dielectric constant and the loss tangent of the cellulose derivative binders are of the same order of FR4. The circuit parameters used in the simulation are reported in Table 1. S-parameters (S_{12} and S_{22}) are not plotted since they are close to S_{21} and S_{11}, respectively. Measured (dashed line) and model-derived fitted data (solid line) of the transmission coefficient are compared in Fig. 6 for the graphene-filled gap 25wt.% and 33wt.%. Both magnitude and phase are analyzed. No phase differences can be appreciated between the two percentages of graphene, while a reduction (absolute value) in S_{21} can be observed when increasing graphene weight fraction. This effect may be due to the increase in percolative paths, confirmed by a reduction in the sheet resistance. Even if not reported, as expected from the previous result, S_{11} decreases when increasing the weight fraction. Overall good agreement

Table 3: Graphene weight fraction 33% Electrical model parameters

R_s kΩ	R_g kΩ	C_g pF	L_g pH	R_{gl} Ω	C_{gl} pF	R_{gr} Ω
0.207	1	0.032	15.8	28	0.085	28

C_{gr} pF	R_{in} Ω	C_{in} pF	R_{out} Ω	C_{out} pF	C_{pp} pF
0.085	81	0.216	71	0.22	0.24

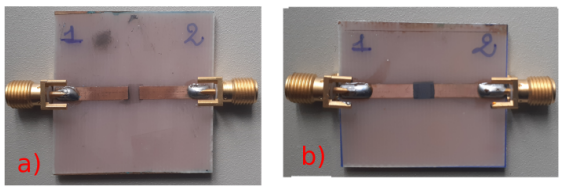

Figure 4: Microstrip with unfilled-gap (a) and filled with graphene-based ink (b).

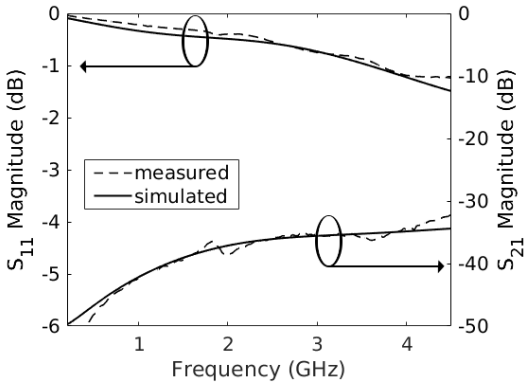

Figure 5: Binder-filled gap: measured reflection and transmission coefficient (dashed line) and simulated (solid line).

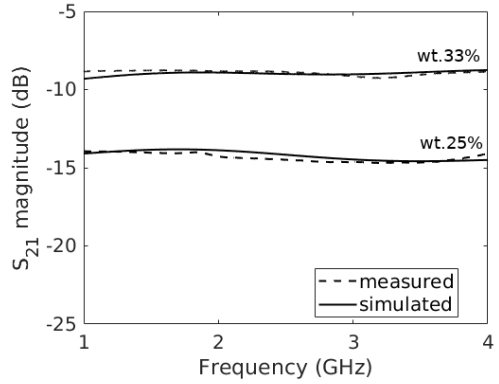

(a)

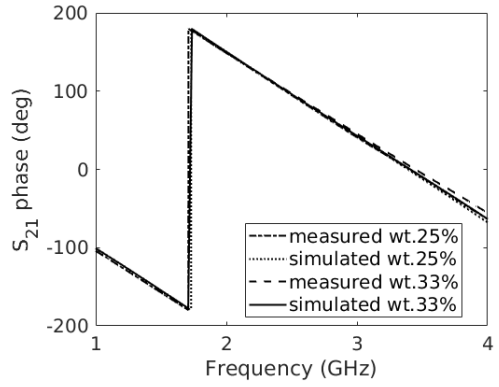

(b)

Figure 6: Graphene-filled gap 25 wt.% and 33wt.%: measured transmission coefficient (dashed line) and simulated (solid line). (a) Magnitude (b) Phase.

is observed between the measurements and the circuit model over the range 200 MHz to 4.5 GHz. Between the measured data and the fitted data a difference lower than 1 dB is obtained for both the transmission coefficient (Fig. 6a) and the reflection coefficient (not reported here). The results obtained in this work and the results of other graphene-based ink depositions made with screen-printing technique are listed in Table 4. The values of DC sheet resistance, modeled (Z_{sim}, corresponding to R_s in Fig. 3) and measured (Z_{meas}), are not directly comparable because the composition of the inks, annealing temperature and thicknesses are different. A common feature is that the sheet resistance values decrease with the increase of the weight percent of graphene nanoplatelets. In [16, 19] the sheet resistance of GNPs inks with different graphene weight fractions is compared in the microwave range. It is shown that the screen printed number of layers influences the electrical properties as well. Graphene percentages taken into account in [19] are lower than those analyzed in this article, leading to much higher resistive effects.

Table 4: Other works based on graphene inks overview

Ink Type	Thickness μm	wt. %	Z_{sim} Ω	Z_{meas} Ω	T °C
EC+teripenol	20	33	207, this work	110, [22]	130
EC+teripenol	20	25	425, this work	440, [22]	130
Copolimer	40	25	–	30, [25]	100
PMMA+organic solvent	20	14	–	180, [19]	260

5. Conclusion

A microstrip line loaded with a graphene insert was fabricated by screen printing and modeled through a lumped-element circuit. Specifically, binder only (ethylcellulose) and graphene-loaded (25 wt.%) were printed on FR4 substrates. Electromagnetic behaviour of both films was simulated with AWR in the 200 MHz to 4.5 GHz range. Measured scattering parameters were fitted by means of *RC* series groups. The additional parallel capacitance inserted in the graphene film model can be ascribed to non-ideal (i.e.leaky) nano-capacitances stemming from the graphene-binder interaction. Simulated and experimental were found to be in accordance with each other (less than 1 dB difference throughout the entire frequency range). This equivalent lumped circuit can be extended to characterize films with different graphene loading. Furthermore, it can be improved and used in full-wave electromagnetic simulations in order to analyze sensing or tunable devices, where graphene is currently modeled by a simple sheet resistance.

6. References

1. W.J. Hyun, E.B. Secor, M.C. Hersam, C.D. Frisbie, L.F. Francis, "High-Resolution Patterning of Graphene by

Screen Printing with a Silicon Stencil for Highly Flexible Printed Electronics," *Advanced Materials*, **27**, January 2015, pp. 109-115.

2. A. Chiolerio, G. Maccioni, P. Martino, M. Cotto, P. Pandolfi, P. Rivolo, S. Ferrero, and L. Scaltrito. "Inkjet printing and low power laser annealing of silver nanoparticle traces for the realization of low resistivity lines for flexible electronics.' *Microelectronic Engineering*, **88**, Aug 2011, pp. 2481-2483.
3. Secor, B. Ethan, L. P. Prabhumirashi, K. Puntambekar, M. L. Geier, M. C. Hersam. "Inkjet printing of high conductivity, flexible graphene patterns." *The journal of physical chemistry letters*, **4**, Apr 2013, pp. 1347-1351.
4. T. S. Tran, N. K. Dutta, N. R. Choudhury. "Graphene inks for printed flexible electronics: Graphene dispersions, ink formulations, printing techniques and applications." *Advances in colloid and interface science*, **261**, Nov 2018, pp. 41-61.
5. A. CM De Moraes, J. Obrzut, V. K. Sangwan, J. R. Downing, L. E. Chaney, D. K. Patel, R. E. Elmquist, M. C. Hersam. "Elucidating charge transport mechanisms in cellulose-stabilized graphene inks." *Journal of Materials Chemistry C*,**43**, Aug 2020, pp. 15086-15091.
6. F. Bonaccorso, Z. Sun, T. Hasan, A. C. Ferrari, "Graphene photonics and optoelectronics," *Nature photonics*, **4**, 9, September 2010, pp. 611-622.
7. P. Savi, K. Naishadham, S. Quaranta, M. Giorcelli, A. Bayat, "Microwave characterization of graphene films for sensor applications," IEEE International Instrumentation and Measurement Technology Conference (I2MTC), May 22-25, 2017, Torino, Italy.
8. D. Lei,Q. Zhang, N. Liu, T. Su, L. Wang, Z. Ren, Z. Zhang, J. Su, Y. Gao, "Self-powered graphene oxide humidity sensor based on potentiometric humidity transduction mechanism," *Advanced Functional Materials*, **32**,10, March 2022, pp. 2107330-1-12.
9. X. Leng,W. Li, D. Luo, F. Wang, "Differential structure with graphene oxide for both humidity and temperature sensing," *IEEE Sensors Journal*, **17**,14, June 2017, pp. 4357-64.
10. Z. Zhu, L. Gancedo, A. J. Flewitt, H. Xie, F. Moussy, and W. I. Milne, "A Critical Review of Glucose Biosensors Based on Carbon Nanomaterials: Carbon Nanotubes and Graphene," *Sensors*, **12**, May 2012, pp. 5996-6022.
11. R. Reghunath, and K. K. Singh, "Recent advances in graphene based electrochemical glucose sensor," *Nano-Structures and Nano-Objects*, **26**, April 2021, pp. 100750-1-18.
12. M. Bozzi, L. Pierantoni, S. Bellucci, "Applications of graphene at microwave frequencies", *Radioengineering*, **24**, Sep 2015, pp. 661-669.
13. Qu, Meijun, J. Song, L. Yao, S. Li, L. Deng, and Y. Yang. "Design of a graphene-based tunable frequency selective surface and its application for variable radiation pattern of a dipole at terahertz." *Radio Science*, **53**, Feb 2018, pp. 183-189.
14. M. Yasir, S. Bistarelli, A. Cataldo, M. Bozzi, L. Perregrini, and S. Bellucci, "Enhanced tunable microstrip attenuator based on few layer graphene flakes," *EEE Microwave and Wireless Components Letters*, **27**, 4, March 2017, pp. 332-334.
15. Wallace, S. Goff, M. C.,et al. "Fully printed and flexible multi-material electrochemical aptasensor platform enabled by selective graphene biofunctionalization." *Engineering Research Express*, **4**, Mar 2022, p. 015037.
16. M. Olszewska-Placha, B. Salski, D. Janczak, P. R. Bajurko, W. Gwarek, M. Jakubowska. "A broadband absorber with a resistive pattern made of ink with graphene nano-platelets." *IEEE Transactions on Antennas and Propagation*, **63**, Dec 2014, pp. 565-572.
17. D.S.L., Abergel, V. Apalkov, J. Berashevich, K. Ziegler, and T. Chakraborty, "Properties of graphene: a theoretical perspective," *Adv. Phys.*, **59**, 2010, pp. 261–482.
18. M. Liang, M. Tuo, S. Li, Q. Zhu, and H. Xin, "Graphene conductivity characterization at microwave and THz frequency," *8th European Conference on Antennas and Propagation (EuCAP)*, April 6-11, 2014, The Hague, Netherlands.
19. K. Pawel, B. Salski, P. Zagrajek, D. Janczak, M. Sloma, M. Jakubowska, M. Olszewska-Placha, W. Gwarek, "Electric Properties of Graphene-Based Conductive Layers from DC Up To Terahertz Range," *IEEE Transactions on Terahertz Science and Technology*, **6**, May 2016, pp. 480-490.
20. A. Chiolerio, S. Porro, S. Bocchini. "Impedance hyperbolicity in inkjet-printed graphene nanocomposites: tunable capacitors for advanced devices." *Advanced Electronic Materials*, **2**, Mar 2016, p. 1500312.
21. O. Sanusi, P. Savi, S. Quaranta, A. Bayat, and L. Roy, "Equivalent circuit microwave modeling of graphene-loaded thick films using S-parameters," *Progress In Electromagnetics Research Letters*, **76**, May 2018, pp. 33-38.
22. S. Quaranta, M. Miscuglio, A. Bayat, and P. Savi, "Morphological and radio frequency characterization of graphene composite films," *C*, **4**, 2, May 2018, pp.32-44.
23. Cadence AWR (2022). MWO_AO_Elements_v22. p.155. Available: https://kb.awr.com/display/awrfaq/Documentation?preview=%2F11894861%2F93356088%2FMWO_AO_Elements_v22_1.pdf&searchId=VXW417SI0.
24. N.H.L. Koster, and R. H. Jansen, "The equivalent circuit of the asymmetrical series gap in microstrip and suspended substrate lines," *IEEE Transactions on Microwave Theory and Techniques*, **30**, 8, Aug 1982, pp. 1273-1279.
25. K. Arapov, E. Rubingh, R. Abbel, J. Laven, G. de With, H. Friedrich. "Conductive screen printing inks by gelation of graphene dispersions." *Advanced Functional Materials*, **26**, Jan 2016, pp. 586-593.

Fabio Peinetti is with Dept. of Electronic and Telecom., Politecnico di Torino, Torino, Italy; e-mail: fabio.peinetti@polito.it.

Simone Quaranta is with CNRISMN, Istituto materiali nanostrutturati, Rome, Italy; e-mail: simone.quaranta@cnr.it.

Patrizia Savi is with Dept. of Electronic and Telecom., Politecnico di Torino, Torino, Italy; e-mail: patrizia.savi@polito.it.